ASCENT, STAGE SEPARATION AND GLIDEBACK PERFORMANCE OF A PARTIALLY REUSABLE SMALL LAUNCH VEHICLE

Bandu N. Pamadi*, Paul V. Tartabini† and Brett R. Starr‡
Vehicle Analysis Branch
Aerospace Systems Concepts and Analysis Competency
NASA Langley Research Center, Hampton, VA

Abstract

An integrated analysis is presented for ascent, stage separation and glide back performance of a small, partially reusable launch vehicle sized for a payload of about 330 lbs to a 150 nm polar orbit. The altitude margin was used a performance metric for the glideback performance. Aerodynamic databases for each of these three phases of flight were developed using a combination of engineering level code, free stream and proximity wind tunnel test data and Euler CFD results. The ascent and glideback trajectories were generated using POST and the stage separation simulation was done using the in-house software SepSim as a front end to the commercially available multi-body dynamic simulation code ADAMS®. The payload to the designated polar orbit was optimized subject to the constraints imposed by stage separation and adequate performance reserve for the glideback booster in addition to the usual ascent trajectory constraints.

Nomenclature

A_N	normal acceleration, g's
α	angle of attack, deg
$\Delta\alpha$	relative difference in angle of attack, deg
C_A, C_N	axial and normal force coefficient
$C_{A,b}$, $C_{N,b}$	base (free flight) axial and normal force coefficient
$C_{A,\text{int}}$, $C_{N,\text{int}}$	interference axial and normal force coefficient
$\Delta C_{A,\delta e}$, $\Delta C_{N,\delta e}$	axial and normal force coefficient increments due to elevon deflection
$\Delta C_{A,\delta c}$, $\Delta C_{N,\delta c}$	axial and normal force coefficient increments due to canard deflection
C_L, C_D	lift and drag coefficients
C_m	pitching moment coefficient
Cmd	command
δ_c	canard deflection, deg
δ_e	elevon deflection, deg
F_N	normal Force, lb_f
γ	flight path angle, deg
h	altitude, ft
k_1	stage separation interpolation constant
k_α, k_q, $k_{\delta e}$	angle of attack, pitch rate and elevon deflection feedback gains
L_{ref}	vehicle reference length, ft
M	Mach number
q	dynamic pressure, psf
σ	bank angle, deg
V	velocity, ft/s
Δx, Δz	relative axial and normal distances during separation, ft

*Senior Aerospace Engineer, Associate Fellow AIAA.
†Aerospace Engineer, Member AIAA.
‡Aerospace Engineer, Member AIAA.

Introduction

A need exists for new small launch vehicles (SLVs) for the deployment of military, civil and commercial satellites either singly or in satellite constellations and architectures. The SLVs must be highly responsive in providing rapid deployment of small payloads at significantly lower launch costs, improved reliability and maintainability. To address these issues, the Vehicle Analysis Branch of NASA's Langley Research Center is conducting system level studies on an in-house concept of a small launch vehicle. This vehicle concept is a three-stage system with a reusable first stage and expendable upper stages. The design is based on the use of low cost pressure-fed LOX/RP engines developed by Microcosm[1] and the slide-in propulsion module concept of Starcraft Boosters Inc.[2] An advantage of this concept is that the entire propulsion system can be removed and serviced off-line and kept ready for a new launch to reduce the turn-around time. This SLV system is designed to place about 330 lbs in a polar orbit at 150 nm.

A schematic diagram of the flight profile is presented in Fig. 1. The reusable booster is designed to stage around Mach 3 and glide back to the launch site. If staging were to occur at a higher Mach number, the booster would experience aerodynamic heating and require a dedicated thermal protection system. The expendable upper stages continue further and a second staging occurs around Mach 15. The unpowered glideback of the reusable booster eliminates the need for an airbreathing propulsion subsystem and avoids associated maintenance and checkouts needed prior to each launch.

The objective of this study is to evaluate the performance of the small launcher for optimum payload delivery to the designated polar orbit subject to the usual ascent trajectory constraints as well as additional constraints to ensure a safe separation of the first stage booster from the upper stages and return the booster to the launch site with adequate performance margins. Even though several studies are reported in literature on optimization of launch vehicle ascent and glide back trajectories, there are very few studies which consider the optimization of such trajectories in an integrated fashion as done in this study. In ref 3, such an integrated approach is used for a two-stage, winged, fully reusable launch vehicle. However, interference aerodynamic data was not used for the stage separation analysis. In this study, the aerodynamic interference effects are included. The booster is allowed to fly at high angles of attack (up to 48 deg) at supersonic speeds during the glide back phase to enhance glide back performance. The altitude margin, which is defined as the height of the booster when it returns to the launch site, is used as a performance metric for the glideback trajectory. The POST (Program to Optimize Simulated Trajectories) was used for generating ascent and glide back trajectories.[4] An aerodynamic separation of the booster from the upper stage vehicle is simulated using in-house code called SepSim which is a MATLAB®-based front end to the commercially available Automatic Dynamic Analysis of Mechanical Systems (ADAMS®) solver.[5]

Vehicle Description

The first stage vehicle is a pressure-fed LOX/kerosene, reusable, wing-body booster similar to the Starcraft booster design.[2] A schematic diagram of the small launch vehicle is shown in Fig. 2 and a three-view drawing of the booster is presented in Fig. 3. The glideback booster is named the Langley Glide Back Booster (LGBB). The main wing of the LGBB has a leading edge sweep of 45 deg, a dihedral of 6 deg and an 81-deg leading edge strake. The wing is sized to provide a 150 kt landing speed. The vehicle also features forward located canards, full-span split elevons on the main wing, a conventional centerline vertical tail and rudder that can function like a speed-brake when needed. The booster propulsion system consists of four 50-Klb thrust (vacuum), pressure-fed engines based on Microcosm designs.[1] These engines are assumed to have two-axis gimbal capability for pitch and yaw control during the boost phase. The second stage design mirrors the design of the Microcosm Sprite core stage and uses two pressure-fed 22.8-Klb thrust engines. The third stage design also mirrors the Microcosm Sprite third-stage design and the engine used is based on the qualified Microcosm pressure-fed 5.5-Klb-thrust motor. The characteristics of the small launch vehicle are presented in Table 1.

Table 1. Characteristics of Small Launch Vehicle

Characteristic	Booster	Second Stage	Third Stage
Gross Weight, lbf	88,727	23,859	4,080
Dry Weight, lbf	28,915	3,166	1,104
Number of Engines	4	2	1
Thrust per engine (vacuum), lbf	50,000	22,402	5,490
ISP per engine (vacuum), sec	275.0	303.1	298.2
Engine Exit area, ft^2	3.34	6.79	1.70

The schematic diagram of the attachment of the upper stages to the booster is presented in Fig. 4. The

booster is attached to the upper stages at two points. The forward and aft attachment points (joints) are located at 13.75 ft and 37.93 ft respectively from the nose of the upper stage vehicle. Prior to the release, the forward joint is assumed to be a fixed support and the aft joint is assumed to permit rotation in pitch. The gap between the two vehicles is estimated to be about 1.25 ft at the forward joint and 0.5 ft at the aft joint. These struts and the gap measurements are similar in geometry to the Shuttle Orbiter and External Tank attachment system except that the rear strut has a pivot linkage that allows the rotation of the booster relative to the upper stages upon release. This separation sequence is similar to that used in Ref. 3.

The estimated mass properties at staging, that is, when the booster propellants are depleted and the upper stages are fully loaded with propellants are presented in Table 2.

Table 2. Mass Properties of Vehicles at Staging

Property	Upper Stage	Booster
Mass, slugs	867.6708	897.9814
Total thrust	0	0
x_{cg}, ft	35.0883	37.9375
y_{cg}, ft	0	0
z_g, ft	0	0
I_{xx}, slugs-ft^2	344.0	16,000.0
I_{yy}, slugs-ft^2	167,000.0	304,000.0
I_{zz}, slugs-ft^2	167,000.0	314,000.0

Development of Aerodynamic Databases

The aerodynamic databases used in this study include only longitudinal static aerodynamic coefficients (3 DOF). The dynamic or damping derivatives and the lateral/directional aerodynamic coefficients are not included in these aero databases. A brief description of each aero database follows.

First Stage Ascent Aerodynamic Database

The first stage ascent aerodynamic database covers the Mach range of 0.2 to 4.5, angle of attack from –4 to 20 deg. The aerodynamic coefficients of the stack (upper stages and the glide back booster) were assumed to be the sum of those for the isolated core and the isolated booster. In other words, the mutual interference between the two vehicles was ignored in the ascent aerodynamic database. The aerodynamic coefficients of the upper stage core were generated using Aerodynamic Preliminary Analysis System[6] (APAS) which is an interactive computer code for engineering-level estimates of aerodynamic coefficients from subsonic to hypersonic speeds. The aerodynamic data on isolated booster was generated as discussed a little later. A discontinuous variation of C_L, C_D and C_m occurs around Mach 3 (Figs. 5 to 7) because slender body/panel (Unified Distribution Panel) methods were used for $M < 3$ and impact (Hypersonic Arbitrary Body Program) methods for $M \geq 3$.

Second and Third Stage Ascent Aerodynamic Database

The ascent aerodynamic coefficients of the second stage (Mach 3 to 15) and third stage (Mach 10 to 25) were generated using APAS. The angle of attack ranged from –4 to 20 deg. Since the second and third stage vehicles (cores) are axially symmetric, the data provided for positive angles attack can be used to derive that of negative angles of attack.

The effect of power was ignored in generating the aerodynamic coefficients in the aero databases. However, corrections to base drag for power-on effect were estimated using Space Shuttle flight test data[7] and were implemented separately in POST simulations.

Glideback Booster Aerodynamic Database

The booster glideback aerodynamic database covers Mach range from 0.2 to 4.5, angle of attack from –4 to 48 deg, elevon deflections from –30 to 20 deg, canards from –30 to 20 deg and speedbrake at 90 deg. For developing the booster glideback aero database, APAS was used for Mach 0.2 to 1.25 and the data from Langley's Unitary Plan Wind Tunnel (UPWT) tests for Mach 1.6 to 4.5. A 1.75% scale model of LGBB was used in the UPWT tests. The angle of attack ranged from –4 to 48 deg. The APAS estimations from Mach 0.2 to 1.25 and for angle of attack up to 20 deg were anchored using the test data on the 1% scale model of the LGBB in the NASA Marshall Space Flight Center's (MSFC) Aerodynamic Research Facility (ARF) and Euler CART-3D computations provided by NASA's Johnson Space Center (JSC). The APAS data above 20 deg. angle of attack for Mach 0.2 to 1.25 are not anchored in this study. The APAS methods for subsonic and low supersonic speeds are based on linear potential flow theory and do not consider viscous/boundary layer effects and stall phenomena. In view of this and pending further validation, the data from 20 deg to 48 deg for Mach 0.2 to 1.2 are provided as place holder and will be used with care and caution in glide back trajectory simulation.

The lift, drag and pitching moment coefficients for the first stage, second stage and the glideback booster are

presented in Figs. 5 to 13. The aerodynamic coefficients for the third stage (Mach 10 to 25) are not presented here. The third stage aerodynamic coefficients are very close to that of the second stage because the two configurations are very similar and APAS predictions are not very sensitive to changes in Mach number above 10.

Stage-Separation Aerodynamic Database

The stage-separation or the proximity aerodynamic data for the small launch vehicle configuration used in this study are not available. The aerodynamics of multi-bodies in stage separation environment is quite complex and is dominated by multiple shockwaves and their reflections. At present, validated engineering level or CFD methods for developing stage-separation aerodynamic database are still not available. Recently, NASA Langley Research Center, with participation from MSFC, JSC and Ames has initiated a comprehensive effort to develop stage-separation tools and methodologies. This effort was started under the 2nd Generation Reusable Launch Vehicle program which was an element of NASA's Space Launch Initiative (SLI) and is currently supported by NASA's Next Generation Launch-Vehicle Technologies (NGLT) program. The stage-separation tool development activity includes wind tunnel testing, CFD and engineering level tools. The LGBB configuration is used in a belly-to-belly, bimese version as the baseline configuration in this tool development activity. The belly-to-belly arrangement of two winged vehicles like the LGBB represents a possible "worst" case of mutual aerodynamic interference in a TSTO (Two Stage To Orbit) configuration due to the complex structure of the wing and body shock waves. In view of this, it serves as a good test case for the stage-separation tool development activity. To date, NASA-Langley has conducted Mach 3 stage separation wind tunnel tests on the LGBB-Bimese configuration in Langley's UPWT and Mach 6 tests in the Langley's 20-Inch Mach 6 tunnel. NASA-MSFC has conducted tests in ARF at Mach 3 (Ref. 8). Currently, tests on the LGBB bimese configuration at Mach 10 are underway in Langley's 31-Inch Mach 10 tunnel. In the absence of a better alternative and for the purpose of this study, the available stage-separation Mach 3 test data on the bimese configuration of the LGBB is used to develop the stage-separation aerodynamic database for the small launch vehicle.

The longitudinal stage-separation aerodynamic coefficients depend on the relative location of the two vehicles as characterized by three variables Δx, Δz and $\Delta\alpha$. A sketch showing the relative locations of the two vehicles during staging is shown in Fig. 14. The dependence of stage-separation aerodynamic coefficients on Δx, Δz and $\Delta\alpha$ is in addition to their usual dependence on Mach and α. In this study, the Mach number is assumed to be constant during the staging.

In the Mach 3 stage separation wind tunnel tests, one LGBB vehicle designated as the orbiter (upper stage) was always held at a fixed location and at $\alpha = 0$. The second vehicle designated as the booster was moved in x and z-directions and was held at two values of angles of attack, 0 and 5 deg. The control deflections were not considered in the stage separation tests conducted at Langley and MSFC. Thus, wind tunnel test data is available for orbiter at $\alpha = 0$, $\Delta\alpha = 0$ and $\alpha = 0$, $\Delta\alpha = 5$ deg. For the booster, test data is available at $\alpha = 0$, $\Delta\alpha = 0$ and $\alpha = 5$ deg, $\Delta\alpha = 5$ deg. These data are presented in Figs. 15-18. The data for other values of α and $\Delta\alpha$ are not available. It is assumed that incremental coefficients for $\Delta\alpha = 0$ and $\Delta\alpha = 5$ at other angles of attack are same as those at $\alpha = 0$ and $\alpha = 5$. With this assumption, the available interference aerodynamic test data along with interference free (freestream) wind tunnel test data on the LGBB at Mach 3 and APAS estimates for the upper stages at Mach 3 are used to populate the stage-separation aero database. It is quite possible that the actual stage-separation aerodynamic coefficients for the small launch vehicle configuration are very different from those used in the present version of the stage separation aero database, because, unlike the bimese orbiter, the upper stage (core) vehicle has no wings. In view of this, the results of the stage-separation simulations presented in this paper are considered to be exploratory in nature.

The Mach 3 UPWT test data does not cover sufficiently large values of Δx and Δz so that it transitions smoothly from stage separation (proximity) data to freestream (interference free) data. In view of this, following approach is used to transition smoothly from the stage-separation aero database to the free stream aero database for each vehicle as they move apart.

$$C_A = k_1 C_{A,b} + (1 - k_1) C_{A,\text{int}} + C_{A,\delta e} + C_{A,\delta c}$$

$$C_N = k_1 C_{N,b} + (1 - k_1) C_{N,\text{int}} + C_{N,\delta e} + C_{N,\delta c}$$

$$C_m = k_1 C_{m,b} + (1 - k_1) C_{m,\text{int}} + C_{m,\delta e} + C_{m,\delta c}$$

Here, C_A, C_N and C_m, denote the axial force, normal force and pitching moment coefficients in staging environment, $C_{A,b}$, $C_{N,b}$ and $C_{m,b}$ are basic or interference-free axial force, normal force and pitching moment coefficients, $C_{A,\text{int}}$, $C_{N,\text{int}}$ and $C_{m,\text{int}}$ are the stage-separation

or the proximity aerodynamic coefficients, k_1 is an interpolation constant for transition from the stage-separation aerodynamics ($k_1 = 0$) to the basic aerodynamics ($k_1 = 1$). The transition region is assumed to consist of an inner ellipse and an outer ellipse which are defined empirically. The parameter k_1 is assumed to vary linearly from 0 at the inner ellipse to 1 at the outer ellipse. The control surface increments like $\Delta C_{A,\delta e}$ and $\Delta C_{A,\delta c}$ due to elevons and canard deflections for the glideback booster were used from the basic or freestream aerodynamic data on the LGBB. For the upper stage core, these are zero because it has no aerodynamic control surfaces.

Reference Parameters

The reference parameters for the aero databases discussed above are presented in Table 3.

Table 3. Aerodynamic Reference Parameters

Aero Database	Reference Area, ft^2	Reference Length, ft	Moment Reference Point
First Stage Ascent	435.0	62.5	42.5 ft from nose on the booster axis
Second Stage Ascent	435 .0	62.5	42.5 ft from nose on the core axis
Third Stage Ascent	435.0	62.5	13.3334 ft from nose on the core axis
Glideback Booster	435.0	62.5	42.5 ft from nose on the booster axis
Stage Separation (Separate Databases for Upper Stage and Booster)	435.0	62.5	42.5 ft from nose of each vehicle

Trajectory Simulation and Optimization

Ascent and Glideback

The primary objective of the trajectory optimization was to maximize the payload weight delivered to the designated orbit while assuring a safe stage separation and returning the booster to the launch site with adequate altitude margin to perform terminal area maneuvers. The ascent and glideback trajectory analysis in this paper was performed using the Program to Optimize Simulated Trajectories (POST),[4] a generalized trajectory simulation and optimization code that has been widely used for 30 years to design and analyze trajectories for a range of aerospace vehicles. POST was used to model and optimize the three-degree-of-freedom powered ascent trajectory and the unpowered booster glideback to the launch site. Optimization was performed within POST using NPSOL,[9] a sequential quadratic programming algorithm that utilizes first and second derivative information to optimize an objective function subject to equality and inequality constraints.

The reference mission for the small launch vehicle considered in this study was to deliver a payload around 330 lbs to a 150 nm circular polar orbit. The launch site was assumed to be Vandenberg Air Force Base and the vehicle was launched towards the south to avoid flying over land. The ascent trajectory was optimized by adjusting the time-dependent pitch-angle profile to maximize the weight inserted into the target orbit. The vehicle ascended in a "heads-down" orientation (see Fig. 1) to facilitate booster separation and reduce the likelihood of a collision with the upper stages. The stages were ignited sequentially; that is, the upper stages were not ignited until the previous stage was depleted and a safe stage separation was accomplished. An oblate Earth gravity model was assumed and atmospheric properties and winds were modeled using the 1999 Global Reference Atmosphere Model (GRAM-99).[10]

Both terminal and in-flight constraints were imposed on the optimization process. The terminal constraints required that the final velocity, altitude, flight path angle and inclination match those of the target orbit. In-flight constraints were placed on the peak dynamic pressure ($q_{max} < 1000$ psf) and wing normal force, which was limited to 2.3 times the booster landed weight. Since the wing was designed to handle landing loads up to 2.5g, this reduction in the margin is assumed to account for unexpected loads due to wind gusts that are not accounted for in this study. No limit was placed on the axial acceleration and a pitch trim constraint was enforced during ascent by adjusting the gimbal angles to balance the pitching moment due to vehicle aerodynamics and misalignment between the thrust vector and the center of gravity (c.g). In addition, the dynamic pressure at staging was limited to 300 psf and the angle-of-attack was required to be around 0 deg. These limits were derived from the stage separation requirements that will be discussed in a later section. To ensure that vehicle rates are small at staging, the zero angle-of-attack constraint was initiated 5 sec prior to booster burnout and held until staging. The vehicle position and velocity at staging were used as initial conditions for the SepSim/ADAMS® analysis. The conditions of the booster at the end of stage separation maneuver were used as ini-

tial conditions for the booster glideback trajectory. Similarly, in the ascent trajectory analysis the upper stages were initialized to correspond to those of the upper stages at the end of staging maneuver.

The glideback trajectory was optimized by adjusting the booster's angle-of-attack, bank angle and elevon deflection profiles to maximize its return altitude over the launch site. Maximizing the return altitude provides altitude margin that may be needed to account for off-nominal conditions, dispersions in atmospheric conditions, winds and terminal area energy management (TAEM) constraints. For the purpose of this study, altitude margin is also considered to be a good metric for determining sensitivities and making relative comparisons between different glideback techniques. Future analyses that include trajectory dispersions and realistically model TAEM maneuvers, vehicle guidance and control will be required to ensure that the altitude margin attained in this study is sufficient.

For the glideback trajectory, the in-flight constraints were consistent with those imposed on the ascent trajectory. Specifically, the peak dynamic pressure was bounded at 1000 psf and the normal acceleration was limited to 2.3 g's. During glideback, the aerodynamic moment was balanced using a combination of elevon and canard deflections. The elevon was deflected as a speed brake early in the glideback trajectory to increase drag and aid in arresting the booster's down range and the canard was deflected to balance the associated aerodynamic pitching moment. The angle-of-attack varied with Mach number and was permitted to vary between –4 and 48 deg. However, to avoid going outside the validated aerodynamic database, the upper alpha bound was limited to 20 deg at Mach numbers below 1.4. The elevon deflection could vary between –30 and 20 deg as long as the canard had enough control power to balance the aerodynamic pitching moment. A feedback control scheme was used to modulate the bank angle, which was adjusted according to the heading error (i.e., difference between the vehicle heading and the heading to the launch site). Thus, POST controlled the bank vs. heading error profile. Since the winds had a significant effect on the glideback trajectory, a worst-case month (July) was used to determine the effect of winds on altitude margin.

Stage Separation

The simulation of the staging event was done using the MATLAB® based in-house Separation Simulation (SepSim) tool that provides a convenient front end to the ADAMS® solver. SepSim is being developed as a part of NASA's stage-separation tool development activity described earlier. SepSim is configured for the dynamic simulation of multi-stage launch vehicle staging. It has the capability to model multiple attachment points with specified degrees of freedom, separation forces, closed-loop flight control, actuator dynamics, atmospheric winds, engine plumes etc. It is also configured for performing Monte Carlo studies. Additional information on SepSim is available in Ref. 11.

Visualization of SepSim Simulation Results

The Synergistic Engineering Environment (SEE), a visualization and analysis environment was used to animate the stage separation maneuver. The SEE used geometry models of each stage and the SepSim output to generate an animation of the staging event. The shape of the upper stage plume was generated off-line (outside SEE and SepSim) using a FORTRAN code based on the method presented in Ref. 12. The SEE animation provides an effective means of collision detection or plume impingement. Additional information on the SEE may be found in Ref. 13.

Results and Discussion

Ascent

The optimized ascent trajectory delivered a payload of 322 lbs to the target orbit conditions 384.9 sec after liftoff at an altitude of 911,420 ft, an inertial velocity of 25,409 ft/s and an inclination of 90 deg (Fig. 19). The mated vehicle reached a peak dynamic pressure of 750 psf at 54 sec into flight (h = 32,000 ft, M = 1.37) and flew near the normal force bound (2.3 times the landed weight) for ~40 seconds as shown in Fig. 20. The vehicle had peak axial loads of 3.4-g with the mated configuration and 6.0-g with the upper stage core.

Booster staging occurs 81 sec into the flight at Mach 2.84, an altitude of 82,022 ft, velocity of 2774 ft/sec and a flight path angle of 66.48 deg. These conditions correspond to a staging dynamic pressure of 300 psf. After booster separation, a 132 lb payload fairing was jettisoned 162 sec into flight when the dynamic pressure fell to 0.1 psf. Second stage burnout occurred at 222 sec (h = 503,000 ft, M = 14.5).

During the first stage burn, the angle-of-attack was held at 0 deg 5 sec. prior to staging, and after staging the upper stage (core) was ramped to –20 deg in 3 sec with the engines off to match the results of the stage

separation simulation. After separation the core engines were ignited and gimbaled to return the vehicle to an angle-of-attack of 0 deg in 2 sec at which time the optimal pitch profile was flown. The angle-of-attack profile is shown in Fig. 21. Also shown in the figure is the gimbal angle time history. During the first stage the gimbal angle required for pitch trim peaks at 13.7 deg and is 8.5 deg just prior to staging. Large gimbal angles are required because the c.g. location is offset from the centerline of the booster in the mated configuration and the engines must be gimbaled to align the thrust vector with the c.g. Moreover, since the stages are ignited sequentially, the booster propellant is depleted at booster burnout but the upper stages are still full, resulting in a significant c.g. offset from the booster axis during the first stage. The shift in the gimbal angle profile at staging occurs because the c.g. offset from the centerline is now zero for the upper stage vehicle (core).

Separation

In the present study, only aerodynamic separation was attempted. Separation forces or thrusters were not used. Also, Monte Carlo simulations to evaluate the effects of various uncertainties in mass properties and aerodynamic data were not performed.

At staging, the angle of attack of each vehicle was assumed to be zero. This assumption is mainly due to limitation of stage separation database and was introduced so that the stage-separation simulations remain, as far as possible, within the parameter space covered by the stage-separation database. Further, the dynamic pressure is limited to about 300 psf because the unpowered upper stage is aerodynamically unstable and a higher dynamic pressure accentuates that tendency. For the purpose of stage separation simulations, it was assumed that at t = 0 the booster and upper stages are in a mated condition.

The staging event starts with the release of the forward joint, at t = 0.05 sec. At that time, the booster starts rotating about the aft joint and its angle of attack starts increasing. This separation sequence is similar to that used in Ref. 3. For the purpose of this simulation, when the booster reaches 5 deg angles of attack, the aft joint was released, thus releasing the booster. The trajectory variables of the two vehicles are presented in Fig. 22 and 23 and snap shots from the SEE animation at some selected times are presented in Fig. 24. In these figures, the booster designated as vehicle 1 and upper stages as vehicle 2. The initial conditions used for this simulation correspond to the staging point in the ascent trajectory and are as follows: altitude = 82,022 ft, velocity = 2774.0 ft/sec, M = 2.84, dynamic pressure = 299.9 lbs/ft^2, flight path angle = 66.48 deg.

A simple proportional and derivative (PD) feedback controller using both canard and elevons as control effectors was used to control the booster motion following its release. The schematic diagram of the PD controller is shown in Fig. 25. Even though SepSim permits modeling actuators as first order lag or second order systems, this provision was not implemented in this study. The actuators were assumed to be effective instantaneously. The feedback gains for a commanded booster angle of attack of 10 deg were adjusted by trial and error as $k_\alpha = 1$, $k_q = -1$, $k_{\delta e} = -1$. The canard and elevon biases (Fig. 25) were set to zero. From Fig. 22, we notice that even though the commanded angle of attack is 10 deg, the booster never gets to this value but it is about one body length apart in the z direction by about 3 seconds and the two vehicles are moving away from each other. At this point, the staging process is assumed to be completed and the engines on the upper stages started. It may be noted that the unpowered upper stage is aerodynamically unstable in pitch and without any corrective action, its angle of attack increased in the negative direction. In view of this, it is necessary to redesign the upper stages so that c.g. moves forward and reduces or even eliminates aerodynamic pitch instability. However, this exercise was not done in this study. Once the upper stage engines are on, its pitching motion was controlled.

Glideback

In the optimized glideback trajectory the booster returns to the launch site 356 sec after separation at Mach 0.57 and an altitude of 46,070 ft. The altitude, Mach and flight path angle profiles are shown in Fig. 26. After separation the booster continues to climb and its velocity initially decreases to 770 ft/s until apogee is reached at an altitude of 157,200 ft. After apogee the velocity begins to increase again until it peaks at 1,735 ft/s when the dynamic pressure is large enough to cause the vehicle to decelerate. This change in dynamic pressure is illustrated in Fig. 27, which shows the initial decrease in dynamic pressure from the separation value of 300 psf to less than 10 psf between 25 and 108 sec. During this time the aerodynamic forces have little effect on the trajectory. After 108 sec the dynamic pressure rises but never exceeds 200 psf. Also shown in Fig. 27 is the normal acceleration profile (negative magnitude indicates an upward force on the booster wings), which remains at or below the 2.3 g limit for the entire

glideback. The constraint was enforced by adjusting the angle-of-attack profile, which is shown in Fig. 28. The initial 15 seconds of the profile was tailored to increase the angle-of-attack from 0 to 48 deg without violating the 2.3-g limit on normal acceleration. The booster transitions to the highest possible α value as soon as possible to maximize drag and arrest the booster's down range. As seen in Fig. 28, to stay within the valid portions of the aerodynamic database, α is reduced to 20 deg when the Mach number falls below 1.6 (i.e., the highest value allowed for the M < 1.6 data). This 20 deg angle-of-attack limit is flown for 80 sec at the top of the ballistic arc when dynamic pressure values are less than 10 psf. By 117 sec when dynamic pressure levels have risen and the Mach number has increased past 1.6, the angle of attack is increased back up to 48 deg to further decelerate the vehicle. Once enough slowing has occurred, alpha transitions to lower values where the lift-to-drag ratio is higher. At 146 sec the vehicle rides the 2.3g normal acceleration limit by modulating α for 31 sec after which the optimal angle-of-attack profile is resumed to maximize the final altitude.

Also shown in Fig. 28 is the bank angle (σ) profile. The initial bank angle is 180 deg because the booster was launched in a heads down orientation. At the start of the glideback, while the dynamic pressure is still substantial, the bank angle rapidly transitions to 80 deg to rotate the lift vector away from the full lift-down direction, thus affecting the flight path angle and the apogee altitude reached by the booster. The apogee altitude must be high enough to ensure a sufficient exchange between kinetic and potential energy. Conversely, if the apogee altitude becomes too high, the range from the launch site (and thus the glideback time) will increase to the point where the drag losses become excessive. Once the apogee is passed and the dynamic pressure begins to build up, the optimal bank profile for turning back to the launch site is flown.

The elevon and canard deflection profiles required to trim the vehicle are shown in Fig. 29. For the entire trajectory the vehicle is trimmed and surface deflections remain within their limits at rates below 10 deg/s.

The ground track for the nominal glideback trajectory is shown in Fig. 30. Nearly the entire trajectory is flown over water. The booster travels a maximum total range of 20.3 nm from the launch site. The figure shows that the turn effectively begins near 100 sec and is complete by 250 sec.

Concluding Remarks

An integrated analysis is presented for the ascent, stage separation and booster glideback performance of a partially reusable small launch vehicle sized for a payload of 330 lbs to a 150 nm circular polar orbit. The payload delivered to the designated orbit is optimized subject to a successful first stage separation and adequate performance reserve for the glideback booster. The altitude margin when the booster returns to launch site was used as a metric for the performance of the glideback booster. POST was used for ascent and glideback trajectories and an in-house developed stage separation software called SepSim which provides a MATLAB® based front end to the ADAMS® solver was used for stage separation simulation. Aerodynamic databases were developed for ascent, stage separation and glideback phases using a combination of APAS, freestream and stage separation wind tunnel test data and Euler CFD results. It was found that the actual payload delivered to the designated orbit is 322 lbs. A simple aerodynamic separation of the booster from upper stage vehicle was possible but needed active feedback control using the canards and elevons. In about 3 seconds, the booster was found to have moved away from the upper stage. The glideback booster had an altitude margin of 46070 ft over the launch site. This altitude margin is assumed to be adequate to handle possible off nominal conditions and dispersions.

Acknowledgements

The authors would like to acknowledge David Bose and Nathaniel Hotchko for help in SepSim simulations, Pete Covell and Mark McMillin for geometry and mass properties, Scott Angster and Jim Hoffmann for animation, Kelly Murphy, Bill Scallion for stage separation wind tunnel test data, Wayne Borderlon and Alonzo Frost for MSFC test data, Ray Gomez for JSC Cart 3D results and Anne Costa for paper preparation.

References

1. Wertz, J.R., Biggs, M., and Conger, R.E., *Status of Scorpius Low Cost Launch Services Program*, Paper No. SSC97-X11-5, 11th Annual AIAA/USU Conference on Small Satellites, 1997.

2. Aldrin, Buzz, Davis, H.P., *The StarBooster 200™ System, A Cargo Aircraft for Space,* AIAA/ASME/SAE Joint Propulsion Specialists Conference, June 1999, Los Angeles, CA.

3. Naftel, J.C., Powell, R.W., *Analysis of the Staging Maneuver and Booster Glideback Guidance for a Two-Stage, Winged, Fully Reusable Launch Vehicle*, NASA TP 3335, 1993.

4. Brauer, G.L., Cornick, D.E., and Stevenson, R., Capabilities and Applications of the Program to Optimize Simulated Trajectories, NASA CR-2770, February 1977.

5. *Using ADAMS/Solver*, Mechanical Dynamics, Inc., 1999.

6. Bonner, E., Clever, E., and Dunn, K., *Aerodynamic Preliminary Analysis System II, Part I – Theory*, NASA CR 182076, April 1991.

7. Boyle W.W., and Pace J.P., *Compedium of Flight Vehicle Base Pressure and Base Drag Prediction Techniques, Final Report*, Contract NAS8-34976, Lockheed Missile and Space Company, August 1983.

8. Borderlon, W.J., Jr, Frost, A.L., Reed, D. K., *Stage-Separation Wind Tunnel Tests of a Generic Two-Stage-To-Orbit Launch Vehicle,* AIAA Paper No. 2003-4227.

9. Gill, P.E., Murray, W., Saunders, M.A. and Wright, M.H., "User's Guide for NPSOL (Version 4.0): A Fortran Package for Nonlinear Programming," Systems Optimization Laboratory, Stanford University, Technical Report SOL 86-2, January 1986.

10. Justus, C.G. and Johnson, D.L., "The NASA/ MSFC Global Reference Atmospheric Model – 1999 Version (GRAM-99)," NASA TM-1999-209630, May 1999.

11. Bose D.M., and Hotchko, N., *Stage Separation Simulation (SepSim)-User's Guide*, AMA Report No. 02-37, Analytical Mechanics Associates, Hampton, VA, October 2002.

12. Salas, M.D., *The numerical Calculation of inviscid Plume Flow Fields*, AIAA Paper No. 74-523.

13. Angster, S., *Synergistic Engineering Environment Build II User's Guide Revision E*, AMA Report No. 03-31, Analytical Mechanics Associates, Hampton, VA, August 2003.

14. Pro-Matlab for Sun workstations, The Math Works, Natick, MA, January 1990.

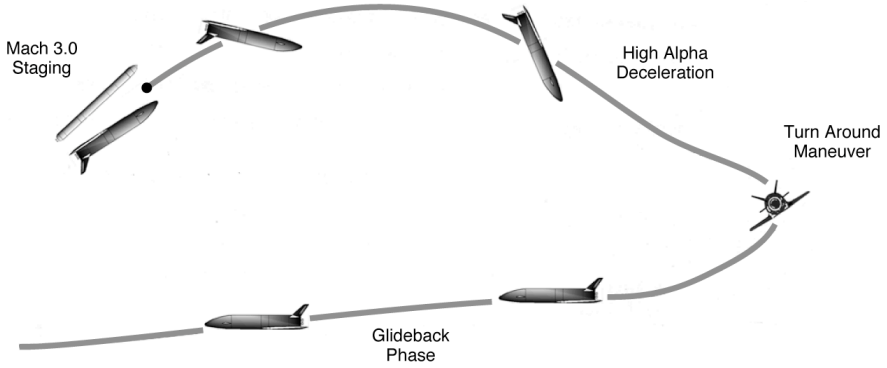

Figure 1. Illustration of the flight profile.

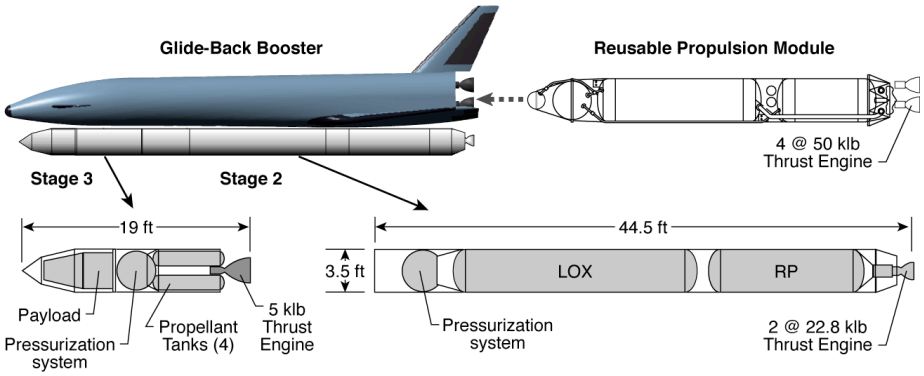

Figure 2. Schematic diagram of the small launch vehicle.

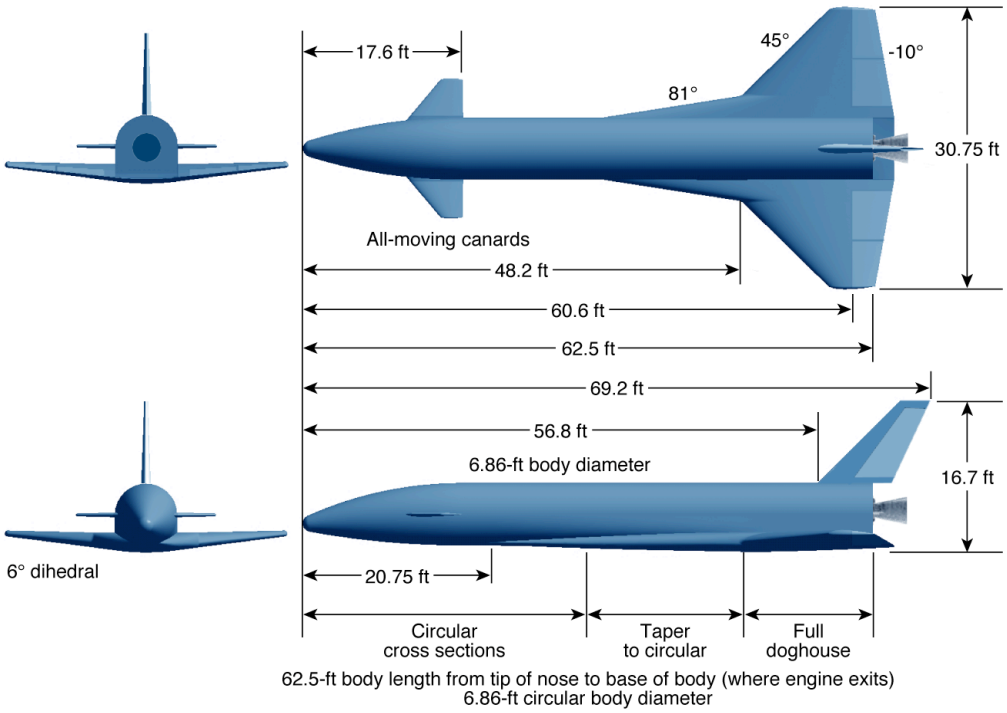

Figure 3. Three-view diagram of the glideback booster.

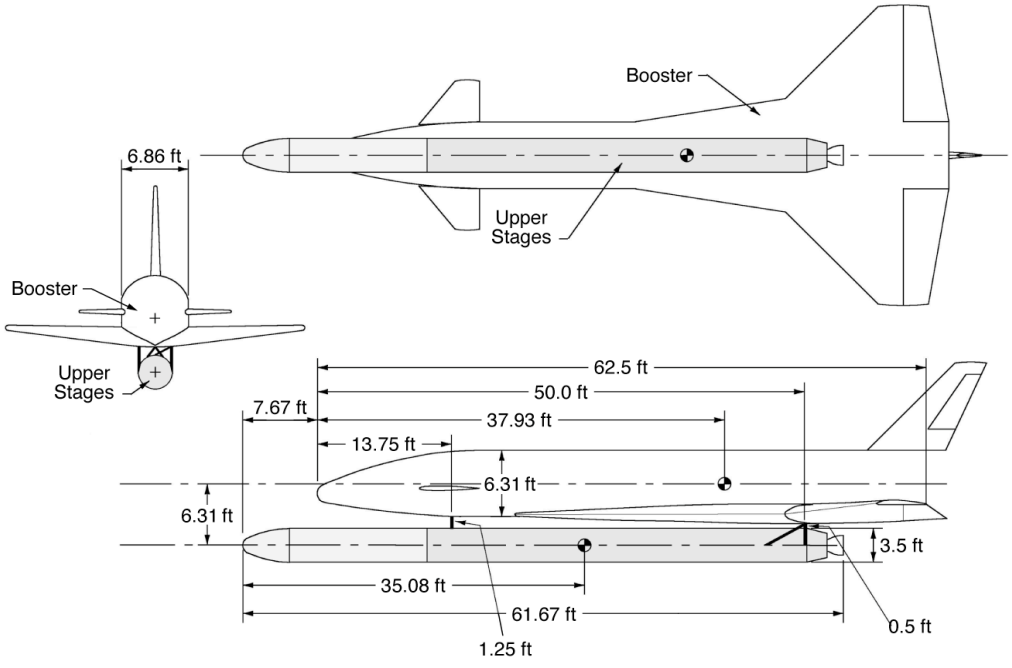

Figure 4. Attachment of the booster to the upper stage vehicle.

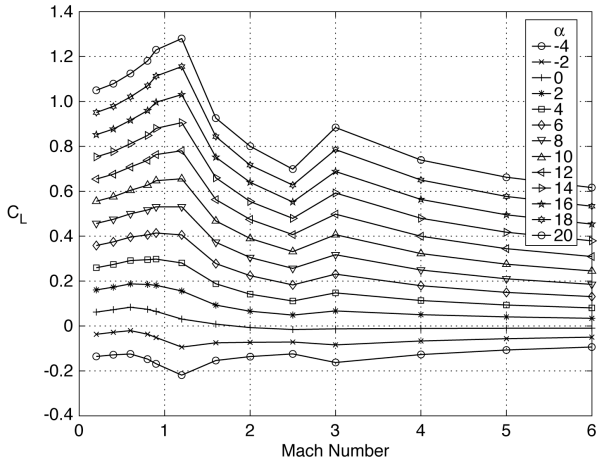

Figure 5. Variation of lift coefficient with Mach and alpha for the first stage vehicle.

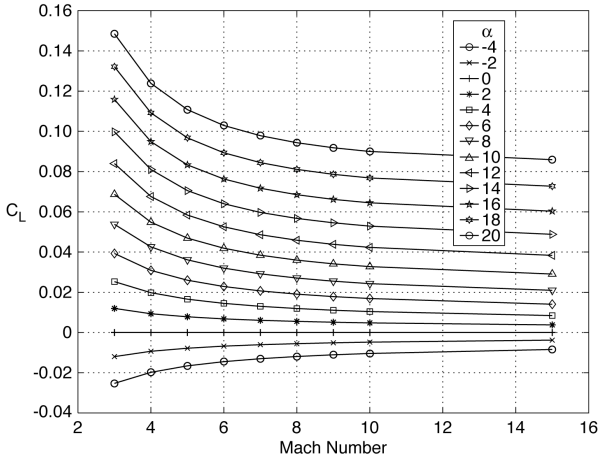

Figure 8. Variation of lift coefficient with Mach and alpha for the second stage vehicle.

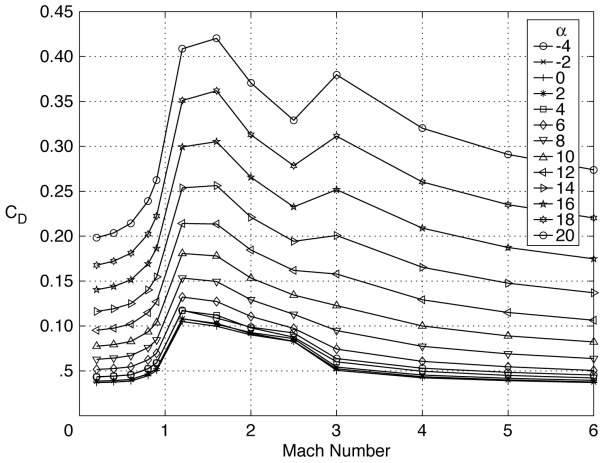

Figure 6. Variation of drag coefficient with Mach and alpha for the first stage vehicle.

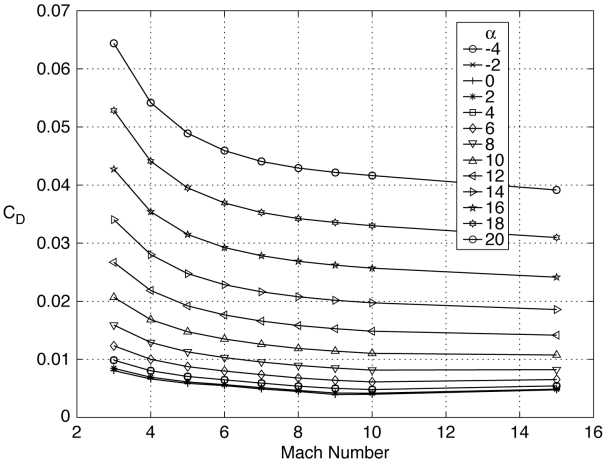

Figure 9. Variation of drag coefficient with Mach and alpha for the second stage vehicle.

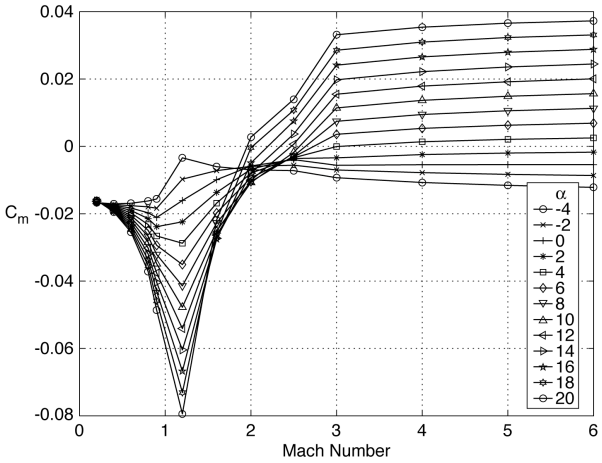

Figure 7. Variation of pitching moment coefficient with Mach and alpha for the first stage vehicle.

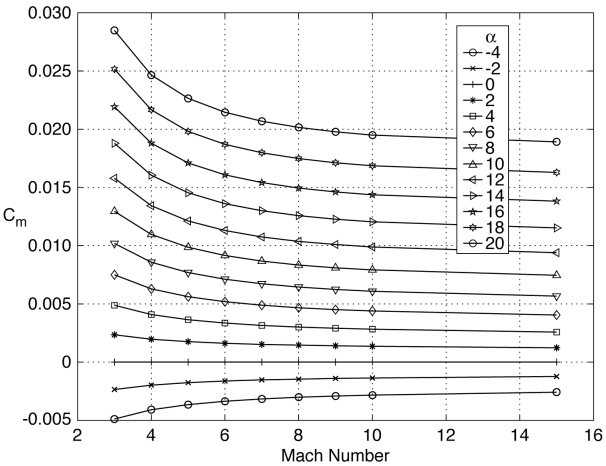

Figure 10. Variation of pitching moment coefficient with Mach and alpha for the second stage vehicle.

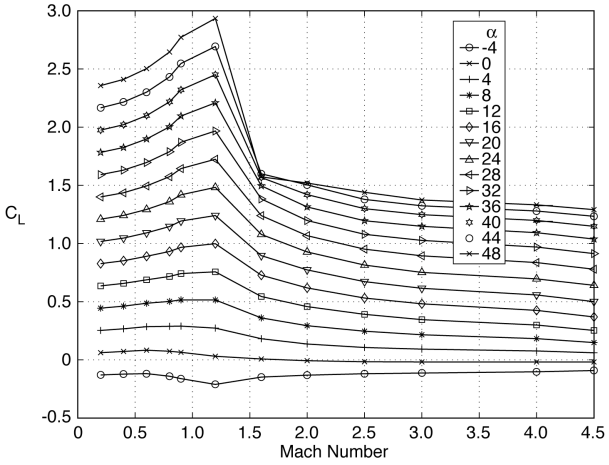

Figure 11. Variation of lift coefficient with Mach and alpha for the glideback booster.

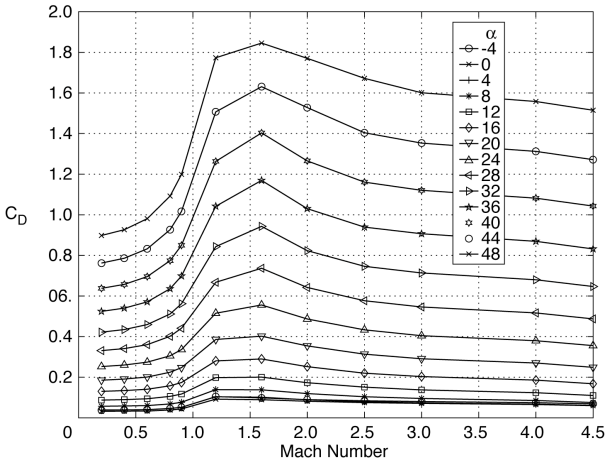

Figure 12. Variation of drag coefficient with Mach and alpha for the glideback booster.

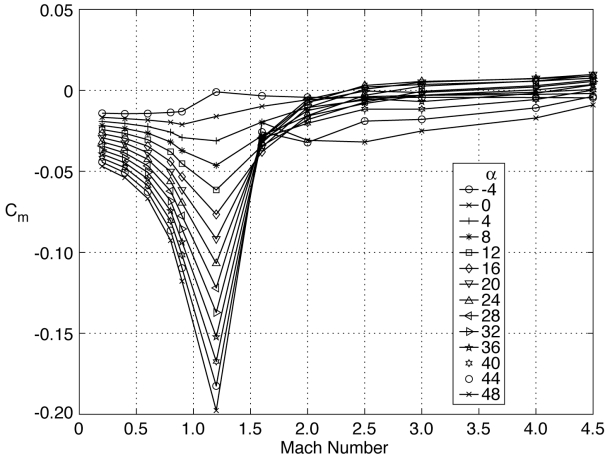

Figure 13. Variation of pitching moment coefficient with Mach and alpha for the glideback booster.

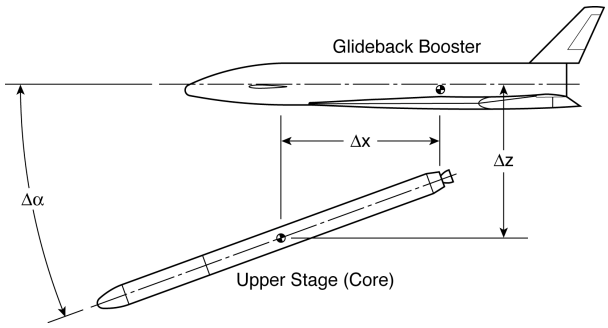

Figure 14. Illustration of relative locations of vehicles during stage separation.

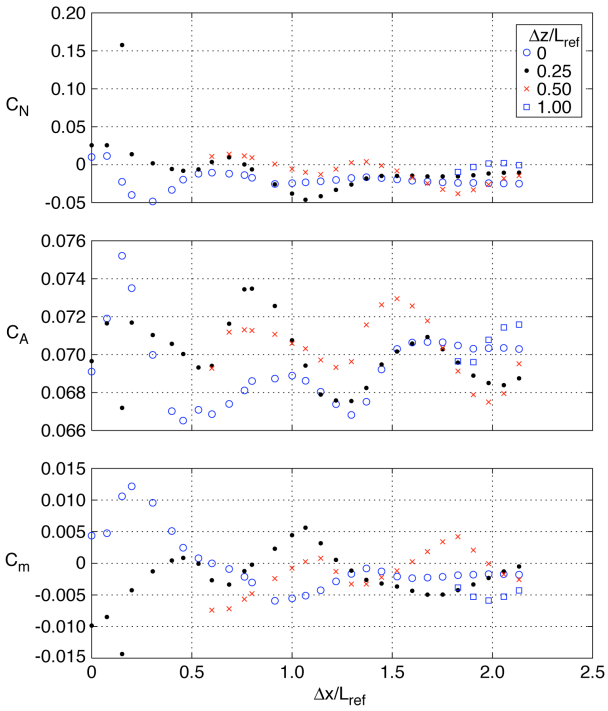

Figure 15. Stage-separation wind tunnel test data for the booster, Mach 3, α = 0, Δα = 0.

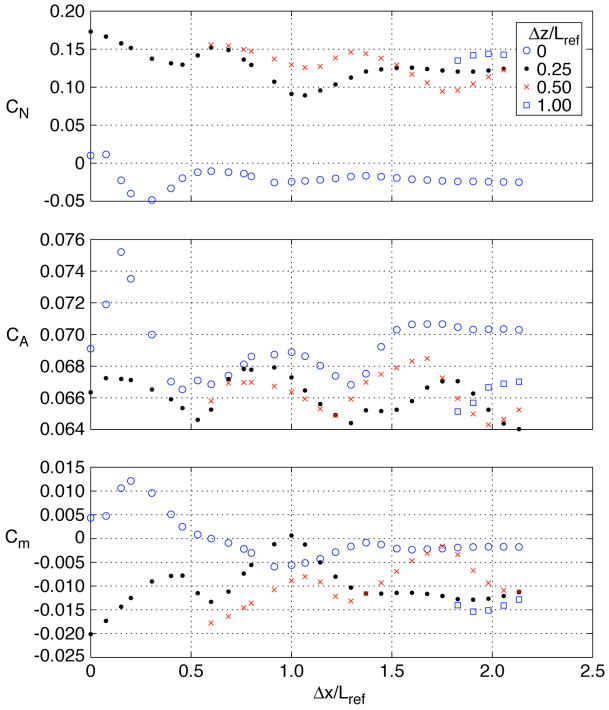

Figure 16. Stage-separation wind tunnel test data for the booster, Mach 3, α = 5 deg, Δα = 5 deg.

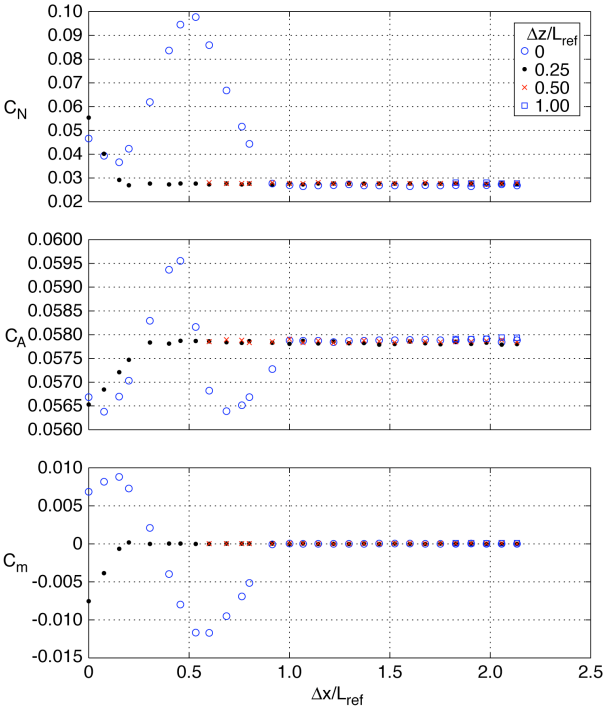

Figure 18. Stage-separation wind tunnel test data for the orbiter, Mach 3, α = 0, Δα = 5 deg.

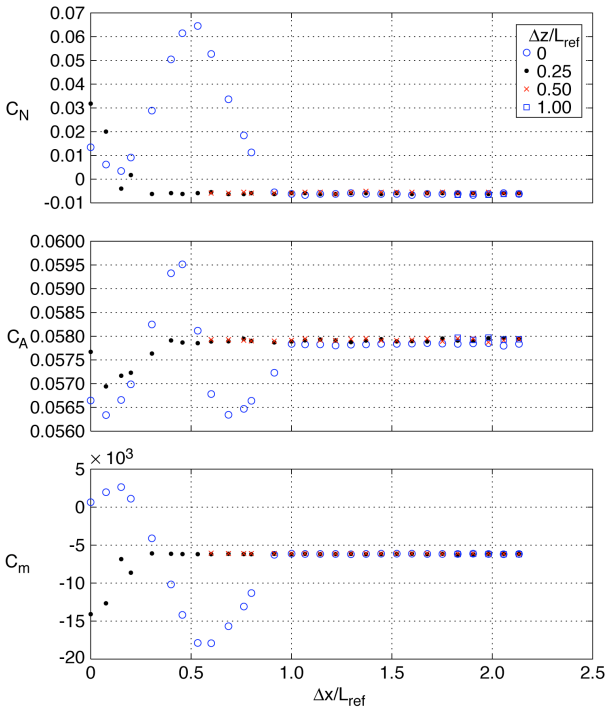

Figure 17. Stage-separation wind tunnel test data for the orbiter, Mach 3, α = 0, Δα = 0.

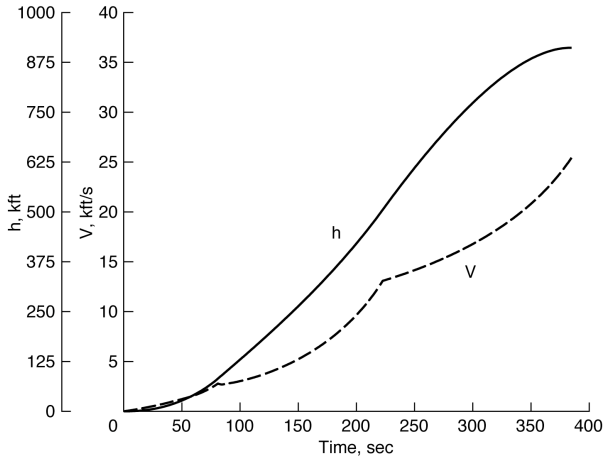

Figure 19. Altitude and velocity profiles for nominal ascent trajectory.

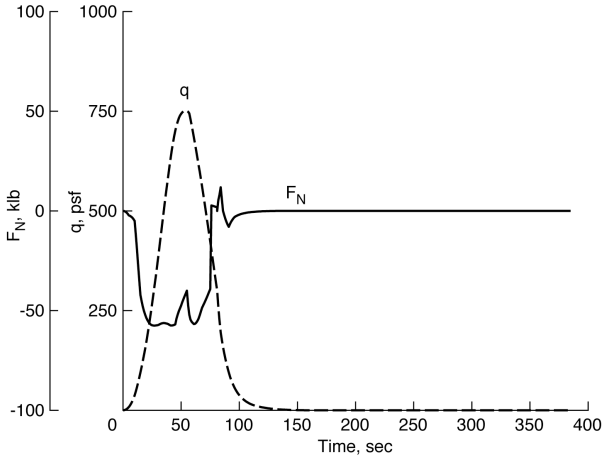

Figure 20. Normal force and dynamic pressure profiles for nominal ascent trajectory.

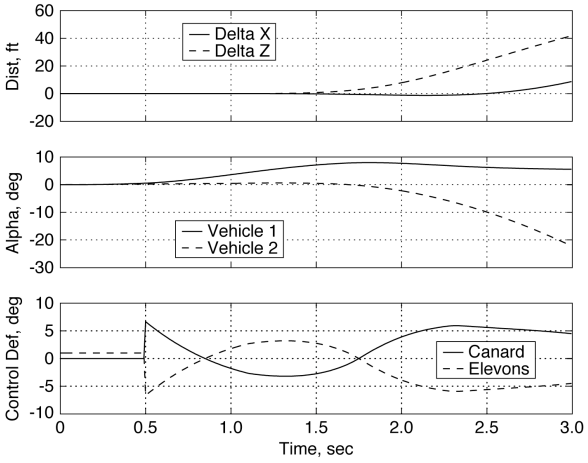

Figure 22. Variation of separation distances, angles of attack and control deflections during stage separation.

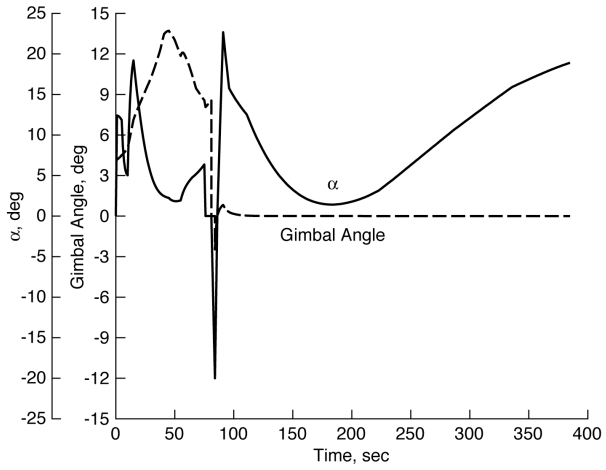

Figure 21. Angle of attack and gimbal angle time histories for nominal ascent trajectory.

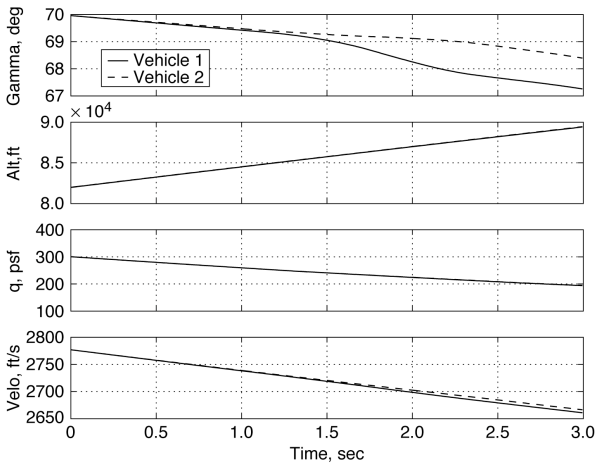

Figure 23. Variation of flight path angles, dynamic pressures and velocities during stage separation.

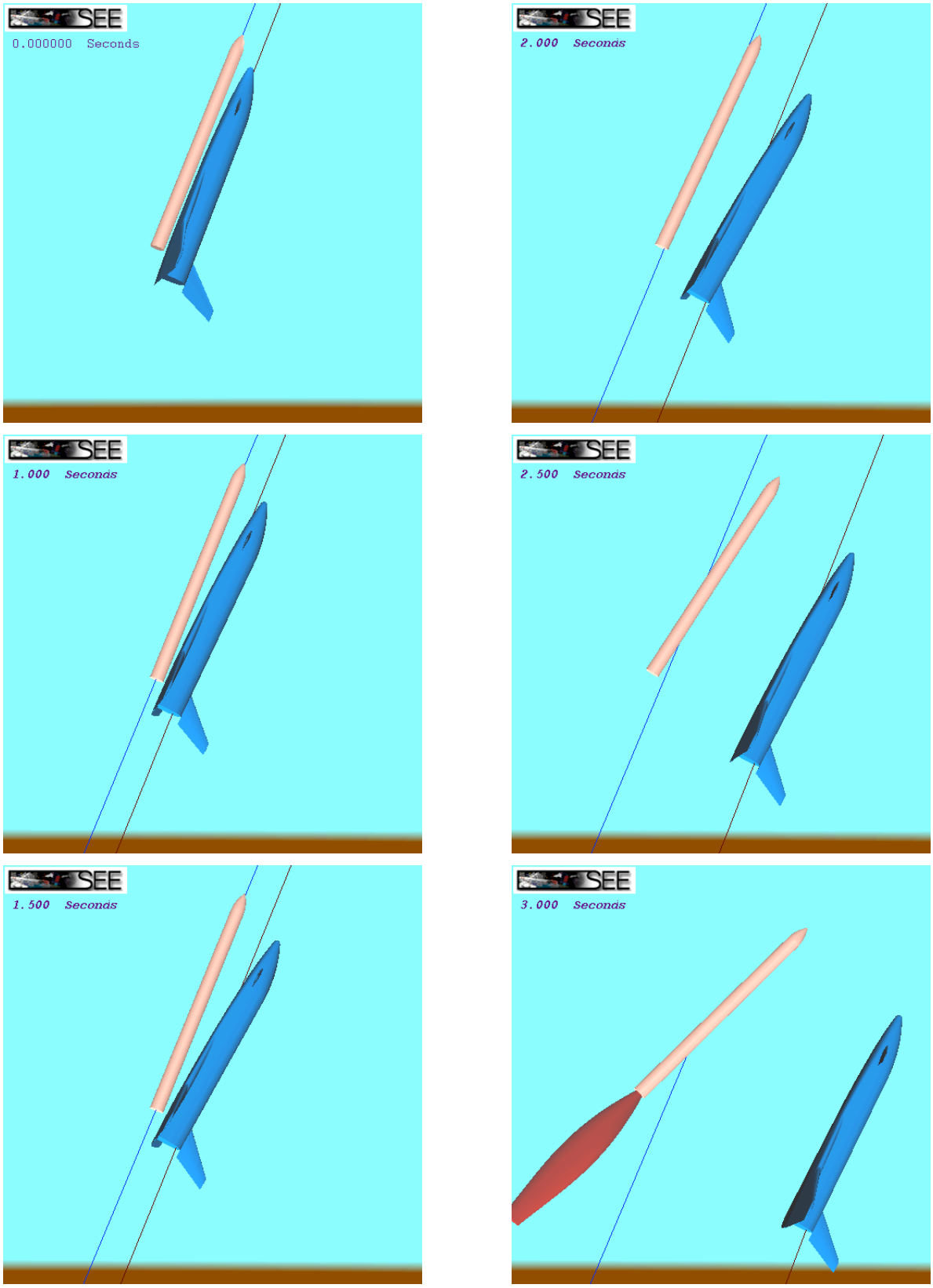

Figure 24. Relative location of vehicles during stage separation.

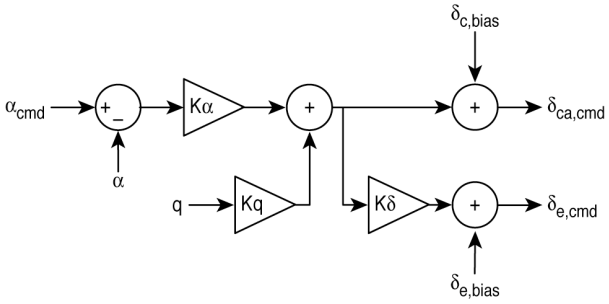

Figure 25. Feedback control system implemented in SepSim.

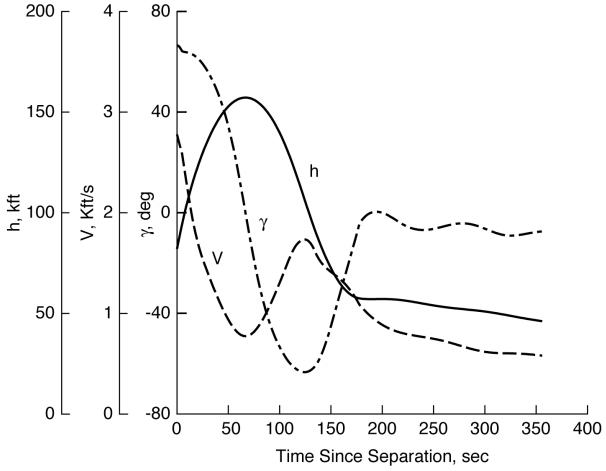

Figure 26. Altitude, velocity and flight path angle profiles for nominal glideback trajectory.

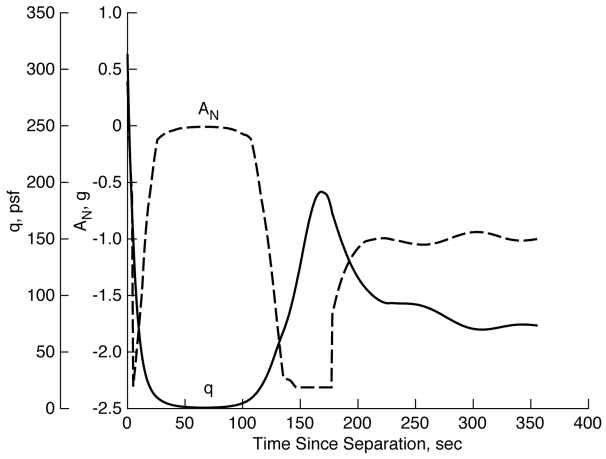

Figure 27. Dynamic pressure and normal acceleration (negative value indicates an upward force on booster wings) for nominal glideback trajectory.

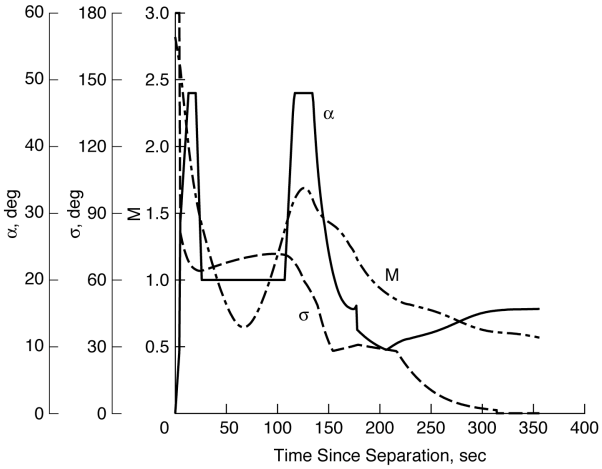

Figure 28. Angle of attack, bank angle and Mach number profiles for nominal glideback trajectory.

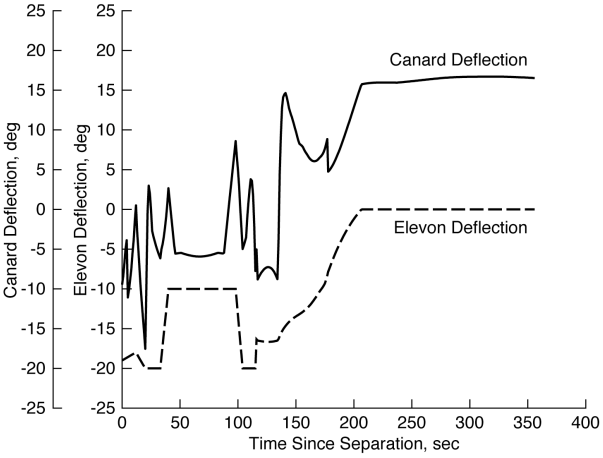

Figure 29. Canard and elevon deflection time histories for nominal glideback trajectory.

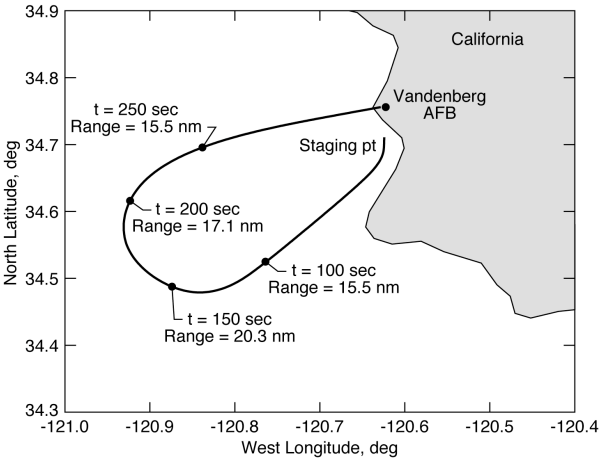

Figure 30. Nominal glideback trajectory groundtrack.